Preprint Title Fabrication of Hafnium-based Nanoparticles and Nanostructures using Picosecond Laser Ablation

Authors Abhishek Das, Mangababu Akkanaboina, Jagannath Rathod, R. Sai Prasad Goud, Kanaka Ravi Kumar, Raghu C. Reddy, R. Ratheesh, Katia Vutova, S. V. S. Nageswara Rao and Venugopal Rao Soma

Publication Date 02 Aug. 2024

Article Type Full Research Paper

ORCID® iDs Abhishek Das - https://orcid.org/0009-0000-4557-4882; R. Sai Prasad Goud - https://orcid.org/0000-0003-1533-0582; Kanaka Ravi Kumar - https://orcid.org/0000-0001-7066-9509; Katia Vutova - https://orcid.org/0000-0002-1300-2369; Venugopal Rao Soma - https://orcid.org/0000-0001-5361-7256

Fabrication of Hafnium-based Nanoparticles and Nanostructures using Picosecond Laser Ablation

Abhishek Das[1], Mangababu Akkanaboina[4], Jagannath Rathod[2], R. Sai Prasad Goud[1], Kanaka Ravi Kumar[1], Raghu. C. Reddy[5], R. Ratheesh[5], K. Vutova[6], S.V.S. Nageswara Rao[1, 3, *], Venugopal Rao Soma[1, 2, *]

[1]School of Physics, University of Hyderabad, Hyderabad 500046, Telangana, India.
[2]Advanced Centre of Research in High Energy Materials (ACRHEM), DRDO Industry Academia – Centre of Excellence (DIA-COE), University of Hyderabad, Hyderabad 500046, Telangana, India.
[3]Centre for Advanced Studies in Electronics Science and Technology (CASEST), University of Hyderabad, Hyderabad 500046, Telangana, India.
[4]Department of Physics, Banaras Hindu University, Varanasi 221005, Uttar Pradesh, India.
5 Centre for Materials for Electronics Technology (C-MET), IDA Phase III, Cherlapalli, HCL (P.O.), Hyderabad 500 051, Telangana India
6 Institute of Electronics, Bulgarian Academy of Sciences, 72, Tzarigradsko Shosse, 1784, Sofia, Bulgaria
Email: S.V.S. Nageswara Rao* - **svnsp@uohyd.ac.in**; Venugopal Rao Soma* - **soma_venu@uohyd.ac.in**

* Corresponding author

Abstract

This work presents a unique and straightforward method to synthesize Hafnium Oxide (HfO_2) and Hafnium Carbide (HfC) nanoparticles (NPs) and fabricate Hafnium (Hf) nanostructures (NSs) on Hf metal surfaces. An ultrafast (picosecond) laser ablation of the Hf metal target was performed in three different liquid media (deionized water (DW), toluene, and anisole) to fabricate HfO_2 and HfC NPs along with Hf NSs. Spherical HfO_2 NPs and nanofibers were formed when Hf was ablated in DW. Hf ablated in solvents like toluene and anisole showed the formation of core-shell NPs of HfC with graphitic shell. All the NPs showed novel optical reflectance properties. The reflectance measurements revealed that the fabricated NPs had a very high and broad optical absorption throughout the UV-Visible-NIR range. The NPs synthesized in toluene especially depicted the best absorption. On the other hand, the successful fabrication of Hf NSs with the formation of picosecond laser-induced periodic surface structures (LIPSS) with low spatial frequency (LSFL) and high spatial frequency (HSFL) orthogonal to each other was also demonstrated. The LSFL and HSFL both showed quasi-periodicity. This article presents a simple way to fabricate HfO_2 and HfC NPs and provides insight into their morphological and optical characteristics.

Keywords

Laser ablation in liquids, nanoparticles, nanofibers, nanostructures, hafnium

Introduction

Hafnium (Hf) is a tetravalent transition metal with compounds showing excellent thermal and optical properties [1–4]. Hf and its alloys are used in nuclear reactors because of their large neutron absorption cross-sections and high melting points [5]. They are also used in submarines due to their corrosion resistance [6,7]. The high refractory property of some of its compounds [2,4] allows it to be used in high-temperature alloys and ceramics. Hf compounds find wide usage in microelectronics due to their high dielectric properties[2]. In recent years, NPs derived from Hf have gained significant interest in biomedical fields due to their superior optical and thermal properties [8] compared to their bulk form. Hf compounds find various uses for their novel properties. The properties vary substantially depending on the size and morphology [1]. Recently, a keen interest has been in synthesizing and studying Hf-based NPs. Depending on the morphology, chemical composition, and quantum confinement effects, NPs can exhibit novel properties, making them applicable for large-spectrum usage [9,10]. Thus, synthesizing the desired morphology is essential for getting the desired application. Generally, the practical techniques for obtaining nanomaterials are the sol-gel method, chemical and physical vapour deposition, hydrothermal method, ball milling, grinding, lithography, etching, laser ablation, etc. [11–14]. The morphology determines the electrical and optical properties, which can vary depending on the synthesis technique [15]. Among the methods mentioned above, Laser ablation in liquids (LAL) is a clean and single-step synthesis method used for obtaining nanomaterials from the bulk source [13,14,16]. It produces fine-size NPs of high purity with minimal or no unwanted side products [14,17], thus making it a valuable candidate for green synthesis [17,18].

In the LAL method, a high-energy pulsed laser is focused on the surface of the source material immersed in a liquid medium. The target material absorbs the pulse energy via the electrons. It transfers it to the lattice, which leads to the expulsion of the surface material as a plasma plume confined due to the extreme pressure created by the surrounding liquid [13,16,19,20]. A cavitation bubble is formed as the energy is transferred to the surrounding liquid from the decaying plasma due to the existing temperature differences between the liquid and the plasma plume, leading to the emergence of a vapour layer with a volume equivalent to the plasma plume [13,16,19,20]. The cavitation bubble collapses due to cyclic expansion and shrinkage, releasing nanoparticles into the surrounding liquid. The formed nanoparticles stay in the liquid as colloidal suspensions or can agglomerate to form a precipitate [6,13,16,19–23]. LAL provides flexibility with the choice of liquid media surrounding the target, from a single pure media to a mixture of liquid media, with a range of target types such as powder, pallets, and well-defined structures and shapes [13,16]. The choice of liquid medium can significantly affect the morphological structure and chemical composition of the obtained NPs. The high energy of the laser pulses sometimes causes a reaction between the surrounding liquid media and ablated target molecules, which may lead to the formation of unusual or non-equilibrium nano-dimensional products [21,22,24,25]. Therefore, the current study intends to understand the role of surrounding liquid media on the laser-ablated Hf-based NPs and NSs. Three different solvents, DW (inorganic and oxygen-containing), toluene (organic and oxygen-free), and anisole (organic and oxygen-containing), have been chosen as ablation media. The Hf target was ablated with a picosecond laser in these three solvents to make three different colloidal solutions of Hf-based NPs. The optical, morphological, and physical properties of the

obtained Hf-based NPs are studied in detail. The morphology of the ablated Hf surface in the three liquids was also investigated.

Experimental details

Materials

Hf Sponge was produced by metallurgical operations involving Solvent extraction, Briquetting, carbo-chlorination, Kroll reduction and vacuum distillation. The sponge samples were further refined by consolidation and refining under a vacuum 3–6×10^{-5} mbar using an Electron Beam (EB) melting furnace having a beam power of 60 kW (ELIT 60) at an accelerating voltage of 24 kV in a water-cooled crucible with feeding mechanism and an extraction system [26]. All the operations were conducted at the Centre for Materials for Electronics Technology (CMET), Hyderabad. These Hf sponges, cut and polished to 10 mm × 10 mm × 2 mm, were used as ablation targets. The pristine target was Hexagonal $HfO_{0.25}$, as confirmed by X-ray diffraction (XRD) [Figure 1(a)]. The elemental composition (Hf: 73.68%, O: 26.32%) was further confirmed by Energy-dispersive X-ray analysis (EDAX) data [Figure 1(b)]. Distilled water with resistivity >18 MΩ-cm was obtained from a Millipore system. Toluene and anisole (spectroscopic grade) were obtained from Sigma Aldrich.

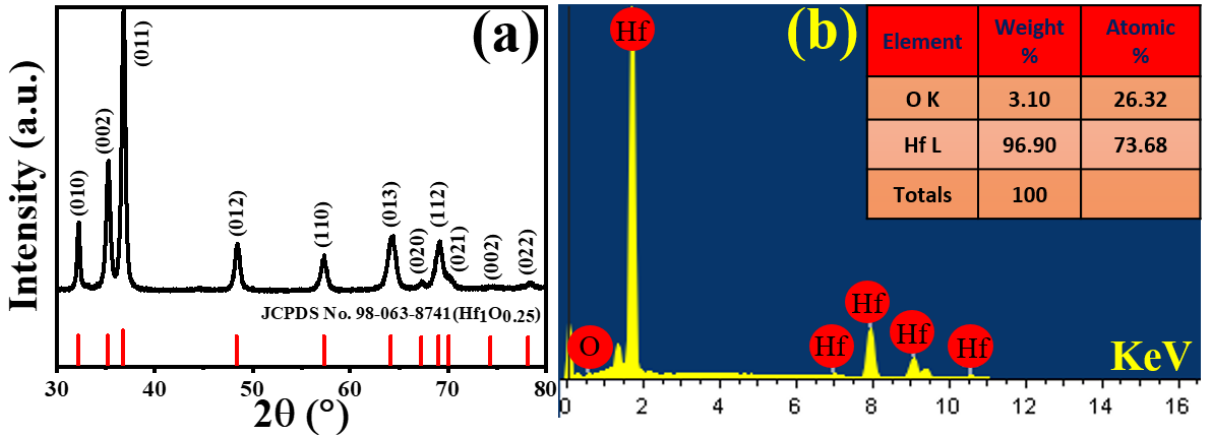

Fig 1: (a) XRD and (b) EDAX data of pristine Hf target.

Synthesis of Nanoparticles and Nanostructures

A linearly polarized picosecond (ps) laser [Nd: YAG, M/s EKSPLA] with a pulse duration of ~30 ps, repetition rate of ~10 Hz, wavelength of ~1064 nm, and pulse energy of ~16.3 mJ was used for the fabrication of the Hf-based NPs and NSs. The ablation was performed in three different liquids, i.e. distilled water (DW), toluene, and anisole. As illustrated in the scheme (Figure 2), the incoming laser beam was focused vertically on the Hf target using a plano-convex lens (f = 80 mm), dipped in 5 mL of liquid-filled glass cell. The liquid surface was about ~ 5 mm above the target surface. The raster scanning was performed at a speed of 0.1 mm/s to ablate an area of 5 mm × 5 mm. This resulted in the formation of Hf surface structures and colloids Hf NPs in the surrounding liquids. A gradual colour change of the liquids initially confirmed this formation of Hf-based NPs in the liquids. The DW turned transparent to turbid

white, while toluene and anisole turned transparent to black (Figure 2). The obtained NPs and NSs are labelled as described in Table 1, according to the liquid in which they were ablated and subjected to various characterizations.

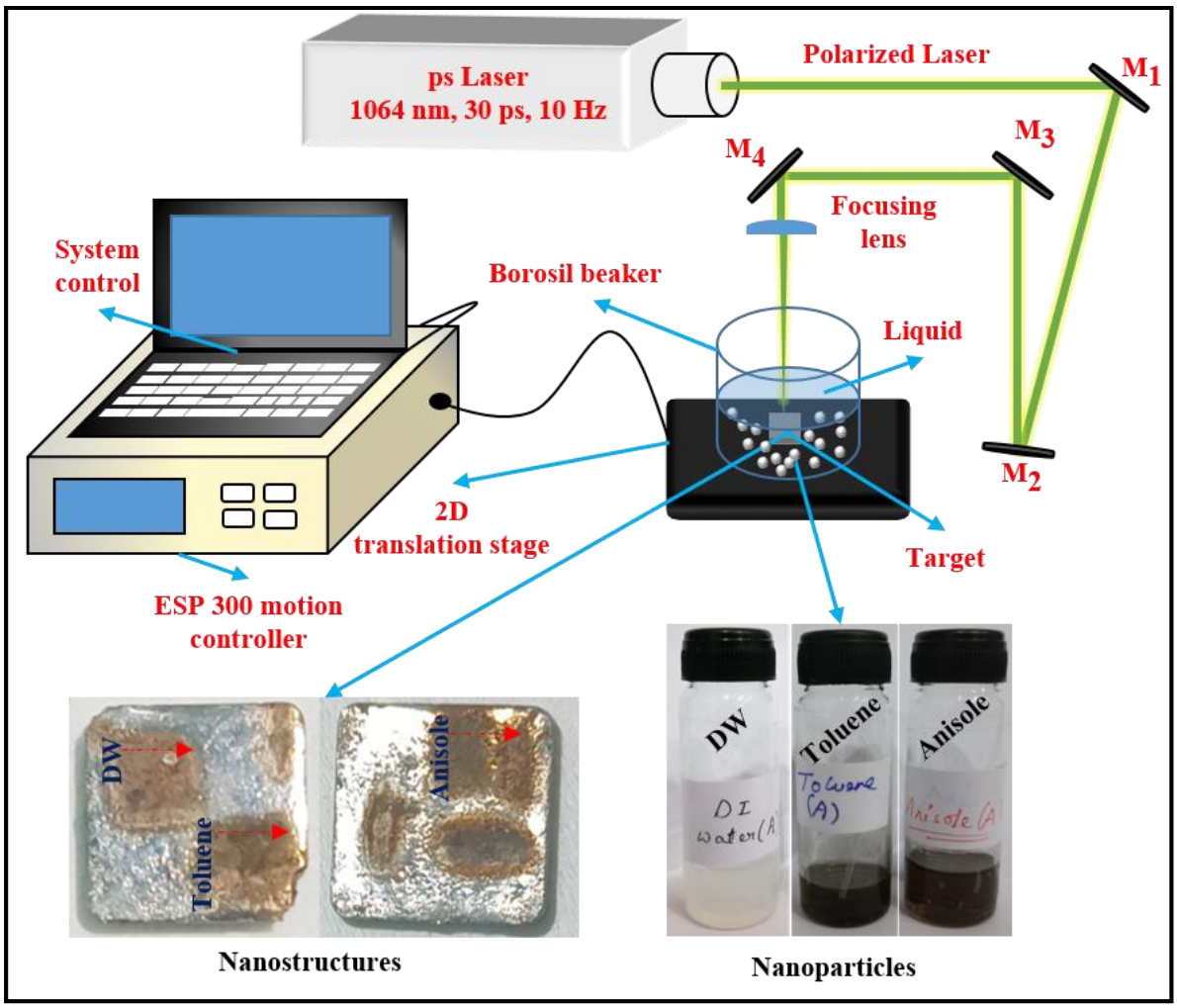

Fig 2: Schematic representation of experimental setup used for picosecond LAL Hf target. (M_n represents mirrors)

Table 1: Labelling of the NPs and NSs according to the liquid media used

Liquids used	NPs	NSs
DW	HfNPs - D	HfNSs - D
Toluene	HfNPs - T	HfNSs - T
Anisole	HfNPs - A	HfNSs - A

Characterization techniques

The synthesized NPs were drop-casted on carbon-coated copper grids to record high-resolution transmission electron microscope (HRTEM) images and Selected area electron diffraction (SAED) patterns using FEI Tecnai G2 S-Twin operating at 200 kV. Further, these NPs were drop-casted on cleaned Si substrates, and their morphology was analyzed using Field emission scanning electron microscopy (FESEM) and its composition by Energy Dispersive X-Ray

Diffractometer (EDX) attached to the FESEM [Model: Carl Zeiss Smart SEM ULTRA 55]. Reflectivity was investigated using a UV-Visible-NIR spectrometer [PerkinElmer Lambda 750]. For photoluminescence (PL) measurements, Horiba LabRAM HR Evolution [Excitation: 325 nm, Lens: 40X, spot size: 1 μm] was used. As mentioned above, the morphology of surface structures formed on the ablated Hf target was thoroughly recorded using an FESEM instrument. Image J software extracted the spatial periodicities and 2D Fast Fourier Transform images (2D FFT) of the Hf surface structures.

Results and Discussion

Nanoparticles

Figure 3 illustrates the TEM images, the corresponding particle size distributions, and the SAED patterns for NPs obtained in DW [Figures 3 (a)-(c)], toluene [Figures 3 (d)-(f)], and anisole [Figures 3 (g)-(i))], respectively. The TEM image corresponding to HfNPs in DW shows the formation of nanofibers along with spherical NPs of diameters ranging from ~ 5 nm to ~ 65 nm [Figure 3(a)]. The formation of nanofibers is consistent with our earlier observations for HfO_2 ablation in DW [27]. Further, the TEM images corresponding to Hf NPs in toluene and anisole [Figures 3(d) and 3(g)] illustrate the formation of spherical particles only. The majority of the NPs have a size distribution in the ranges of 5-40 nm in DW and 5-20 nm in toluene and anisole, respectively, as shown in Figures 3(b), 3(e), and 3(h). The SAED patterns, shown in Figures 3(c), 3(f), and 3(i), indicate that the NPs were polycrystalline. The planes shown in Figure 3(c) for HfNPs - D were found to be (2 0 3), (1 0 3), (1 0 2), and (0 0 2) corresponding to orthogonal Hafnium oxide - Hf_1O_2 (ICDD: 98-008-7456). Whereas, HfNPs - T [Figure 3 (f)] and HfNPs - A [Figure 3(i)] had planes (1 1 1), (0 0 2), (0 2 2), and (1 1 3) corresponding to Hafnium carbide - HfC [ICDD: 98-018-5992]. The observation of HfO_2 in DW and Hf-C in toluene and anisole could be attributed to chemical interactions between the ablated Hf atoms and liquid media. Further, careful observation of high-resolution TEM images revealed the formation of core-shell structure for the particles obtained in anisole and toluene [Figures 4(b) and 4(c)]. In contrast, NPs in DW do not notice such a structure (Figure 4(a)). Shell-like structures in [Figures 4(b) and 4(c)] are indicated with red colour arrows. These shell-like structures are the formation of multi-layered carbon shells around the NPs. Similar formations were noticed in other studies where carbon-rich liquids were used [28–30]. Hence, the d-spacing of the carbon shells was calculated from the zoomed images of shell-like structures shown in [Figures 5(a) and 5(b)], which were found to be around ~0.34 nm, confirming the outer shell to be made of graphite [31–33].

A similar analysis was conducted on the nanofiber-like structures formed when Hf ablated in the DW medium. Figure 6 illustrates the nanofiber location and the SAED pattern for nanofibers [Figures 6 (a-b)] and NPs [Figures 6 (c-d)] formed in DW. A difference can be seen in the crystallinity of the nanofibers and of the NPs. The nanofibers are perfectly polycrystalline (Figure 6(b)). In contrast, in Figure 6(d), the presence of diffused rings for HfNPs - D implies that the NPs exist in a mixed amorphous and polycrystalline state.

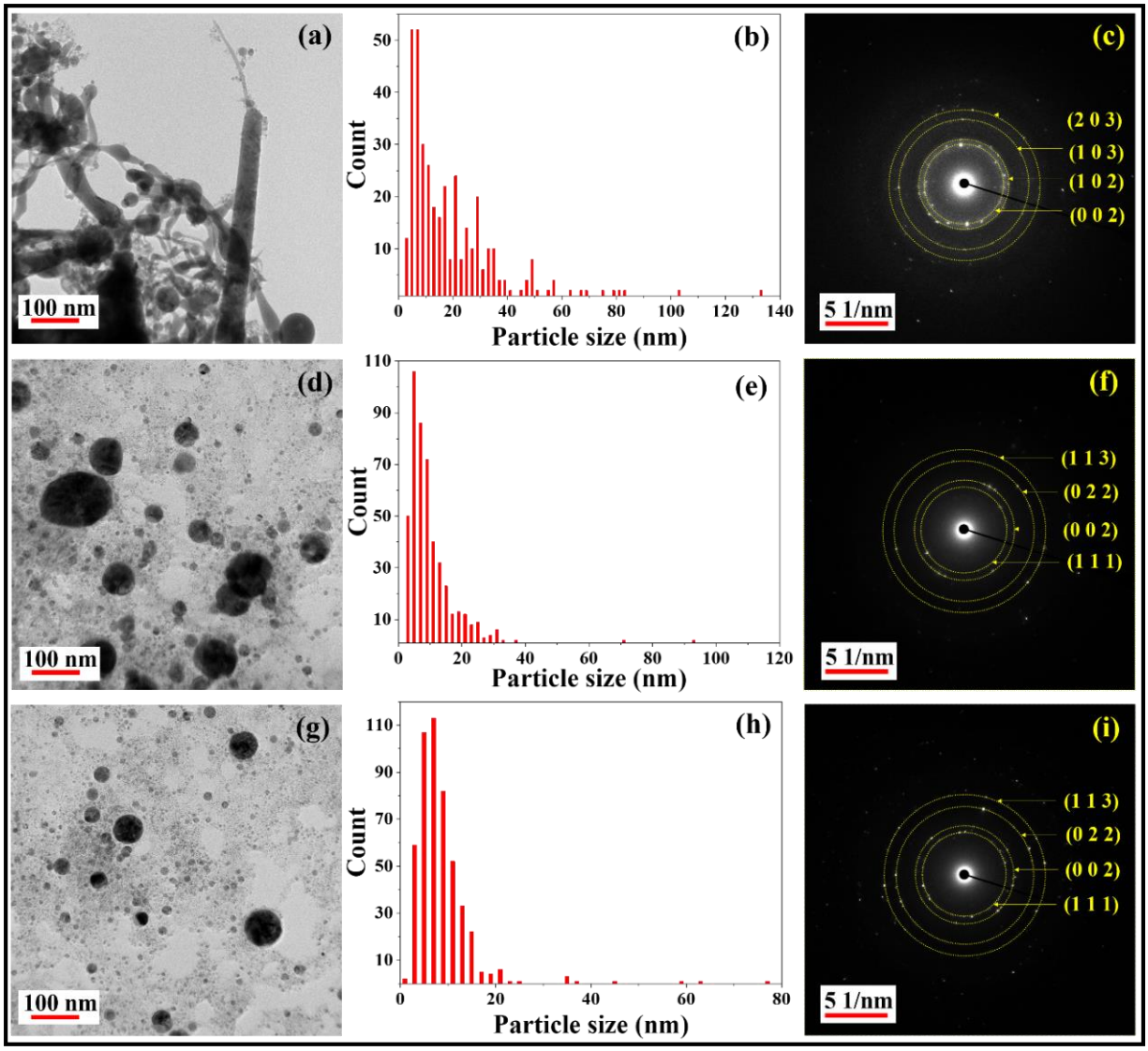

Fig 3: TEM images, the particle size distributions, and SAED patterns of laser ablated NPs in: (a)-(c) DW, (d)-(f) toluene, and (g)-(i) anisole.

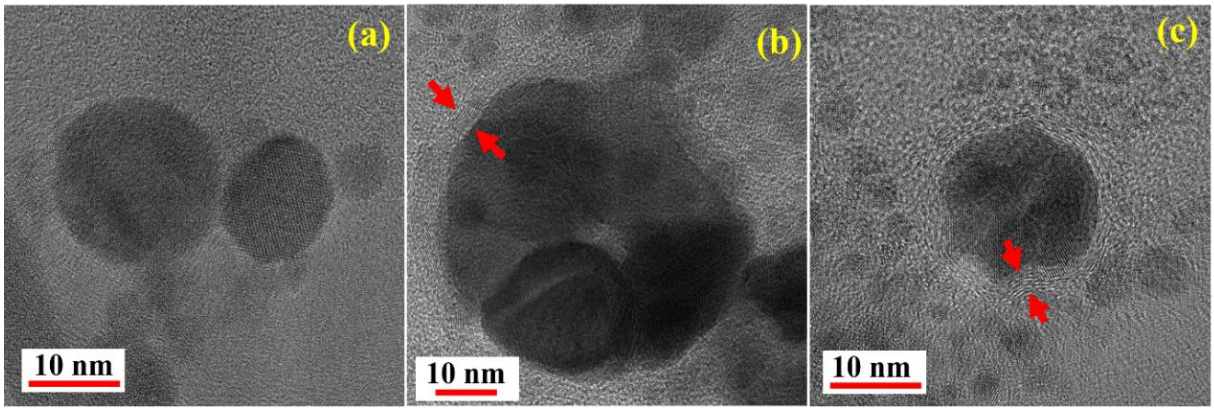

Fig 4: High-resolution TEM images of laser-ablated NPs in (a) DW, (b) toluene, and (c) anisole.

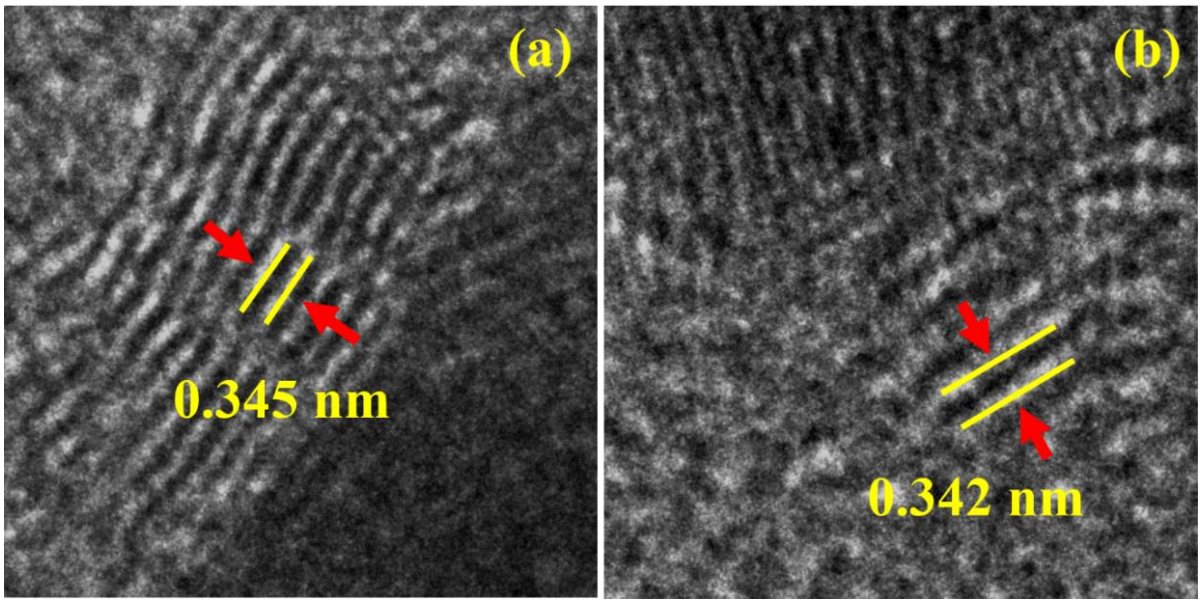

Fig 5: Zoomed TEM images from the shell-like structures shown in Fig. 4(b) and 4(c), respectively, for (a) toluene and (b) anisole (d-spacing of the outer shell is indicated with yellow colour lines).

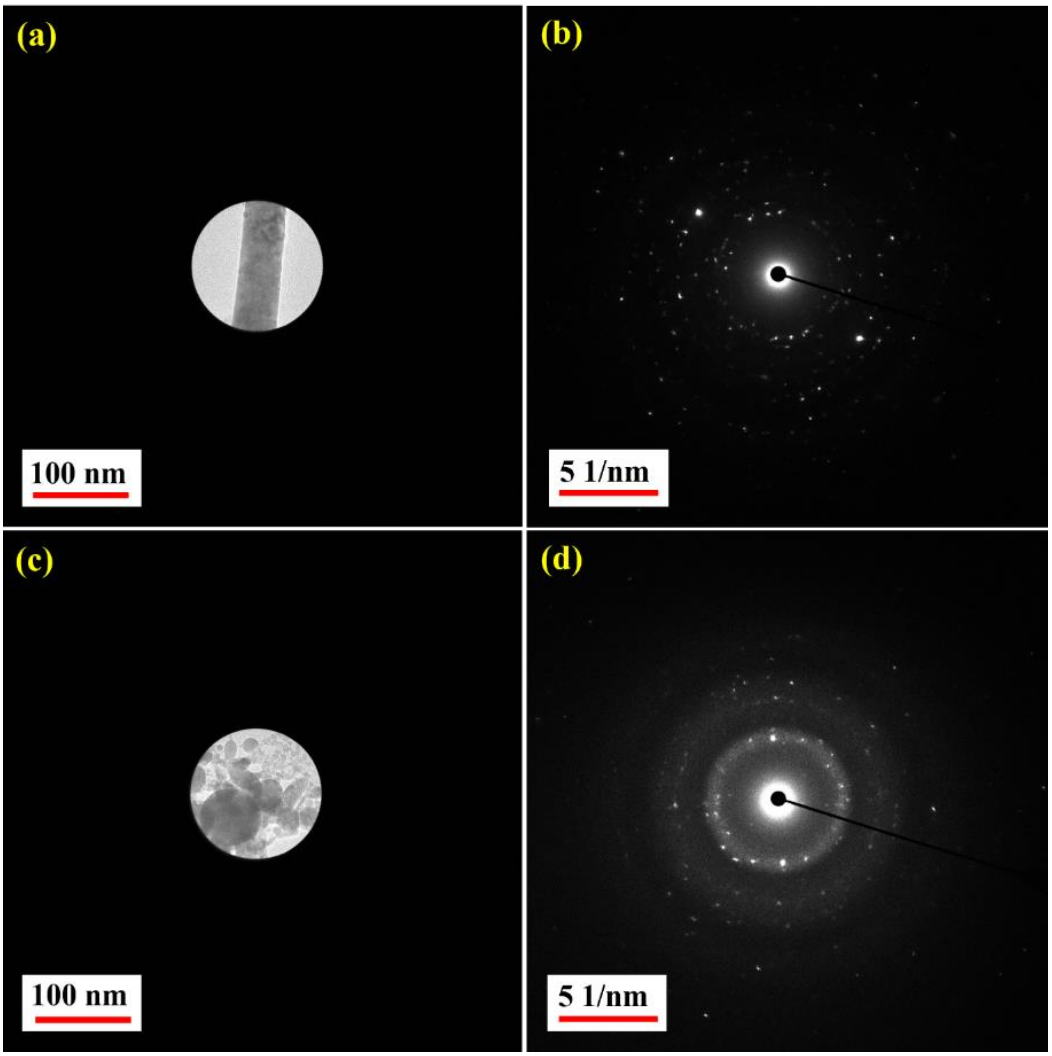

Fig 6: SAED location and pattern for (a)-(b) nanofibers and (c)-(d) NPs obtained in DW.

The formation of HfO_2 NPs in DW along with nanofibers and the observed crystallinity pattern [Figures 6(b) and 6(d)] can be explained by considering the decomposition of the surrounding H_2O molecule due to the laser energy [19,20,34]. This leads to the reaction of oxygen with the Hf^{4+} ion present in the plasma plume formed during the ablation [13,16,19,20,35], leading to the formation of hafnium oxide vapour as the plasma decays. When the plasma plume decays, there is a formation of HfO_2 vapour occupying its volume [13,16,19,20,35]. As the pressure of the surrounding liquid exceeds the vapour pressure exerted by HfO_2, the cavitation bubble collapses, and the vapour rushes through the liquid in the form of a jet [19,20,35]. The lower temperatures of the surrounding liquid lead to the formation of nuclei [19,36,37] with random crystallographic orientation, and they grow using the surrounding hafnium oxide molecules to form crystals [37–39]. These crystals impinge on one another to form a polycrystalline structure [37,40]. As the vapour is rushed out as a jet, these polycrystals assemble [37,41] linearly to form nanofibres. Due to the Brownian motion [42], some nuclei and crystals escape from the jet flow and agglomerate together [37,41,42], leading to the formation of nanoparticles [37]. Some of these nuclei with abundant hafnium oxide molecules around grow like crystals [39,42]. Agglomeration [41] of such crystals leads to the observed polycrystalline state in the NPs [37,40]. The formation of the observed amorphous NPs is due to the suppression of nucleation [37,43]. Thus, a mix of amorphous and polycrystalline states in NPs obtained in DW is seen. The formation of these HfO_2 NPs and nanofibres is responsible for the turbid white colour observed after ablation in DW. The formation of polycrystalline HfC core-shell NPs with graphite shells [30] in toluene and anisole can be explained by the possible reaction of carbon from decomposed surrounding liquid with Hf^{4+} ions in the plasma plume formed during ablation [16,19,20,34]. As the plasma plume decays, its space is occupied by HfC vapour. The pressure difference due to the surrounding liquid causes the cavitation bubble to collapse, and thus, the vapour rushes through the liquid and forms polycrystals, the same as HfO_2 above [13,16,19,20,35,37]. The decomposed surrounding liquid has a carbon-rich environment. As the polycrystals grow, they also act as a nucleus for the carbon molecules to cling onto and self-assemble around them [23,44], leading to the formation of graphite layers, so we get core-shell NPs of different sizes. This formation of the graphite layer might be preventing the formation of fibres. As no oxide of Hf^{4+} was observed, it can be determined that the O^{2+} in the plasma from ($HfO_{0.25}$) didn't react with the Hf^{4+}. It can be explained through reaction equilibrium [19,20,45,46]. The carbon-rich environment near the plasma shifts the equilibrium in favour of the formation of HfC. Thus, the O^{2+} does not react with the Hf^{4+}. The O^{2+} also reacts with C and escapes the liquid as O_2. The black colour observed in toluene and anisole after ablation is due to the formation of HfC core-shell NPs and the decomposition of the surrounding liquid [23,33,47].

Figure 7 illustrates the EDAX data for the synthesized particles in DW, toluene, and anisole. The EDAX spectra of HfNPs - D confirm the presence of hafnium and oxygen elements, as seen in Figure 7(a). The observed atomic percentages of 73.86% Oxygen (O) and 26% Hf [Figure 7(a)] verify the formation of HfO_2. The composition tables for HfNPs - T [Figure 7(b)] and for HfNPs - A [Figure 7(c)] show the presence of carbon (C) and Hf. The composition tables' high atomic% of C indicates the graphitic shell formation around HfC NPs in both toluene and anisole. Figure 8 presents the reflectance data for pristine Si substrate compared to Si substrate coated with HfNPs - D, HfNPs – T, and HfNPs - A via drop-casting with three different angles of incidence (30°, 45°, and 60°) taken over a range corresponding to the

wavelength from 250 nm to 1200 nm covering UV to NIR spectra. The black curve corresponds to the reflectance spectra of the reference pristine Si sample, the red curve is HfNPs - T, the blue curve is HfNPs - A, and the green curve is HfNPs - D. The values of the reflectance % and % reduction in the reflection in UV (λ = 250 nm) and NIR (λ = 1200 nm) spectral regions corresponding to the NPs and different angles of incidence are shown in Table 2. Based on the data, it can be concluded that Hf NPs show a very high and wide optical absorption ranging from UV to NIR. HfNPs - T especially show exceptional performance compared to other NPs with far superior and stable optical absorption. With an increase in angle, a reduction in absorption was observed for HfNPs – D, HfNPs – T, HfNPs - A. A decrease in absorption was observed with an increase in wavelength for a constant angle. The deviation in the spectral

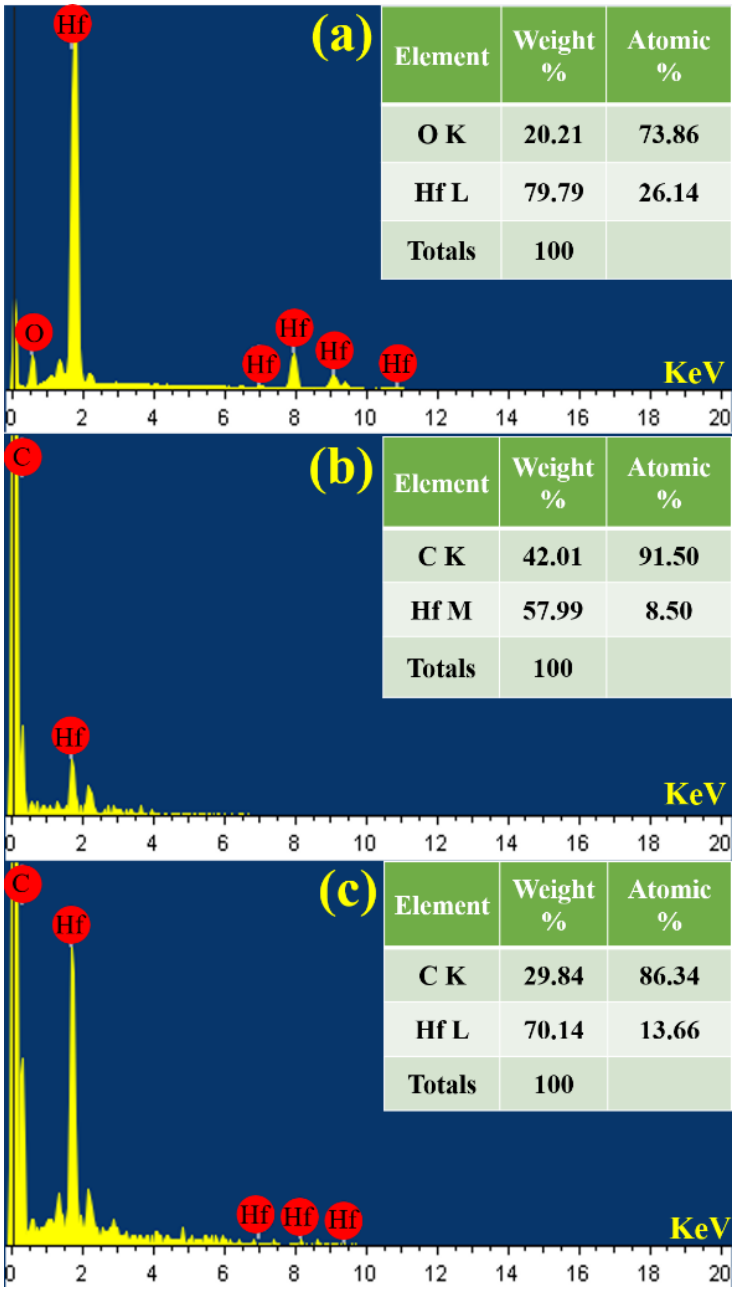

Fig 7: EDAX spectra and the composition of: (a) HfNPs - D, (b) HfNPs – T, and (c) HfNPs - A.

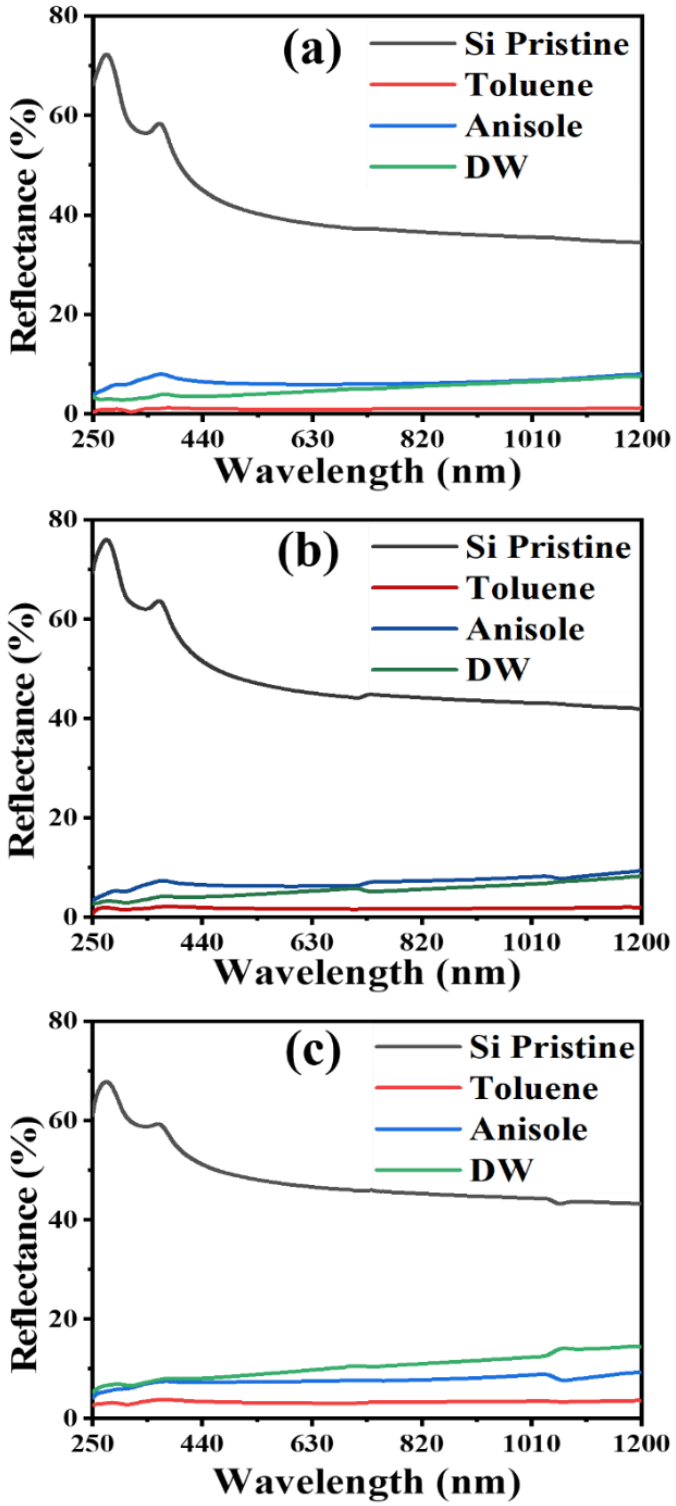

Fig 8: Reflectance spectra NPs drop casted on Si substrate measured at different incident angles: (a) 30˚, (b) 45˚, (c) 60˚. The black curve - the reflectance spectra of the reference Si substrate; the red, blue, and green curves - Hf NPs in toluene, anisole, and DW drop casted on Si substrate, respectively.

pattern of HfNPs - T and HfNPs - A could be due to the presence of O in the polycrystalline lattice of HfNPs – A. The extra O present in anisole compared to toluene might have entered the NPs polycrystalline structure during NPs formation. We can confirm that the oxygen in the anisole molecule is not bonded with the Hf^{4+} ions as no oxide compound was observed from

SAED data for HfNPs - A [Figure 3(i)] as compared to Hf NPs - T [Figure 3(f)]. Thus, the extra O in anisole is likely to be present as an impurity in the polycrystalline structure of the NPs in HfNPs – A and may affect the optical properties of the NPs. Figure 9 shows the PL emission spectra of the laser-ablated NPs in DW, toluene, and anisole. Emission peaks were observed for each of the NPs (Figure 9). The presence of emission peaks indicates the presence of defects in the NPs [48]. The defects may be due to impurities in the lattice structure, imperfect crystallinity of the graphitic layer or the NPs themselves. Further studies are planned to understand the origin of this observed emission peak.

Table 2: Reflectance % and % reduction in reflection in UV and NIR region corresponding to the NPs at different angle of incidence (θ)

Θ (°)		**UV (λ = 250 nm)**	**NIR (λ = 1200 nm)**
		Reflectance % (% reduction of reflectance)	**Reflectance % (% reduction of reflectance)**
30°	Si (Pristine)	66.71 % (-)	34.56 % (-)
	HfNPs – D	3.35 % (94.97 %)	7.83 % (77.34 %)
	HfNPs – T	0.72 % (98.92 %)	1.11 % (96.78 %)
	HfNPs – A	3.35 % (94.97 %)	7.83 % (77.34 %)
45°	Si (Pristine)	70.26 % (-)	41.94 % (-)
	HfNPs – D	3.28 % (95.33 %)	8.23 % (80.37 %)
	HfNPs – T	0.92 % (98.69 %)	1.87 % (95.54 %)
	HfNPs – A	3.28 % (95.33 %)	9.41 % (77.56 %)
60°	Si (Pristine)	61.43 % (-)	43.39 % (-)
	HfNPs – D	5.45 % (91.12 %)	14.55 % (66.46 %)
	HfNPs – T	2.81 % (95.42 %)	3.66 % (91.56 %)
	HfNPs – A	4.27 % (93.05 %)	9.55 % (77.99 %)

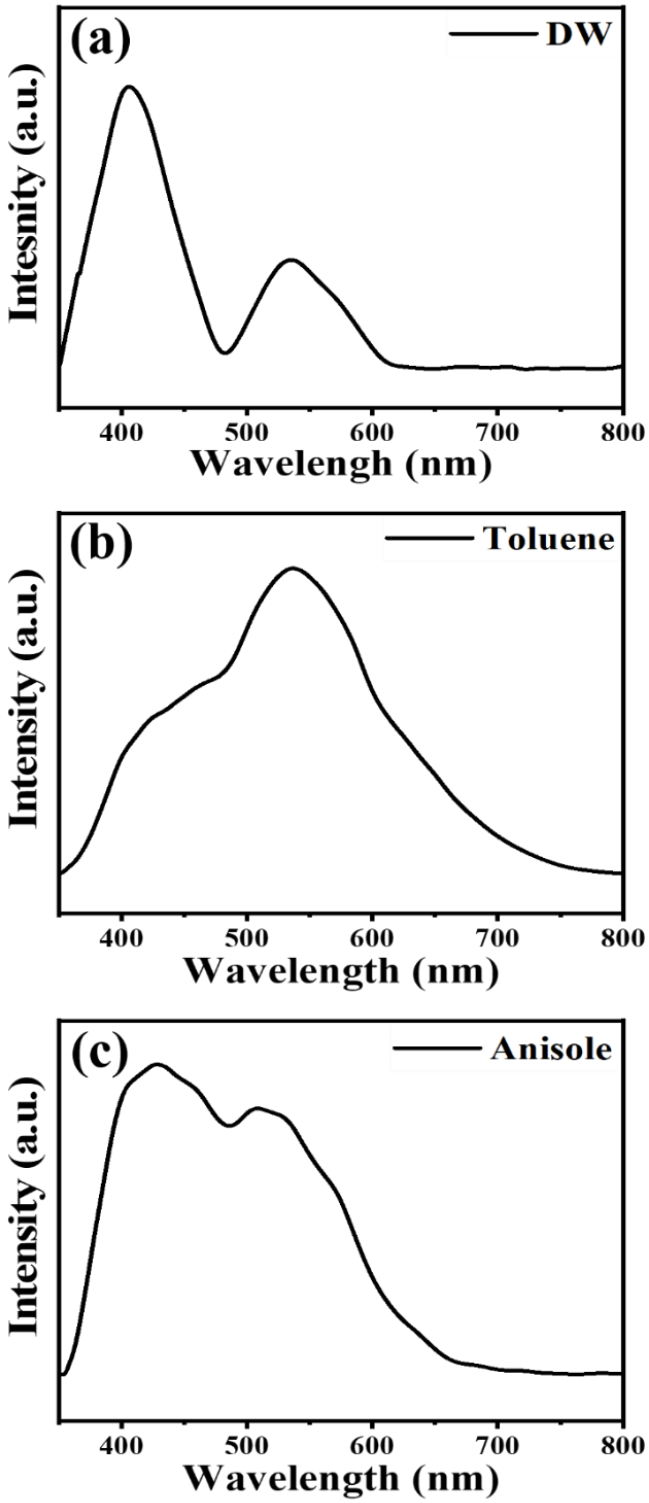

Fig 9: PL spectra for laser ablated NPs in (a) DW, (b) toluene, and (c) anisole.

Nanostructures

Figure 10 illustrates the schemes for the NSs fabrication with picosecond LAL on the Hf target by raster scanning the target. The figure also depicts the LSFL and HSFL formed on the target due to the scanning process. The simultaneous formation of HSFL and LSFL on the Hf target due to LAL was observed in all the respective liquids. The LSFL structures were oriented

parallel to the direction of the laser's scan, and the HSFL is formed in the depressions in LSFL and has a direction perpendicular to the direction of the laser scan. Similar observations regarding the formation of LSFL and HSFL with orthogonal directionality and the plausible mechanism behind their formations are discussed in [49]. Figure 11 illustrates the FESEM images of the laser-ablated NSs and 2D FFT of LSFL with its spatial periodicity for HfNSs - D, HfNSs - T, and HfNSs - A analyzed using ImageJ. Based on the data analysis, it can be concluded that the structures are quasi-periodic and have a sub-wavelength periodicity of $\geq \lambda_L/2$ (λ_L stands for laser wavelength). The quasi-periodicity indicated as D in Figures 11 (b), (d), and (f) was ~ 498.18 ± 39.69 nm for HfNSs - D, ~ 519.485 ± 30 nm for HfNSs - T, and ~ 504.92 ± 63.83 nm for HfNSs - A. On further inspection of the FESEM images of the NSs, the formation of HSFL was observed. Figure 12 illustrates the FESEM image of the HSFL and the corresponding distribution of their feature size in HfNSs – D, HfNSs - T, and HfNSs – A. Based on the data analysis, it can be concluded that the structures show sub-wavelength quasi-periodicity. The observed HSFL had an average feature size between $\lambda_L/11$ and $\lambda_L/8$ for all the corresponding NSs. The feature size for HfNSs - D ranges from ~50 nm to ~150 nm, with an average feature size of 93.5±18 nm, HfNSs – T ranges from ~50 nm to ~200 nm, with an average feature size of 121±36.5 nm, and HfNSs – A ranges from ~50 nm to ~150 nm with an average feature size of 102 ± 24 nm.

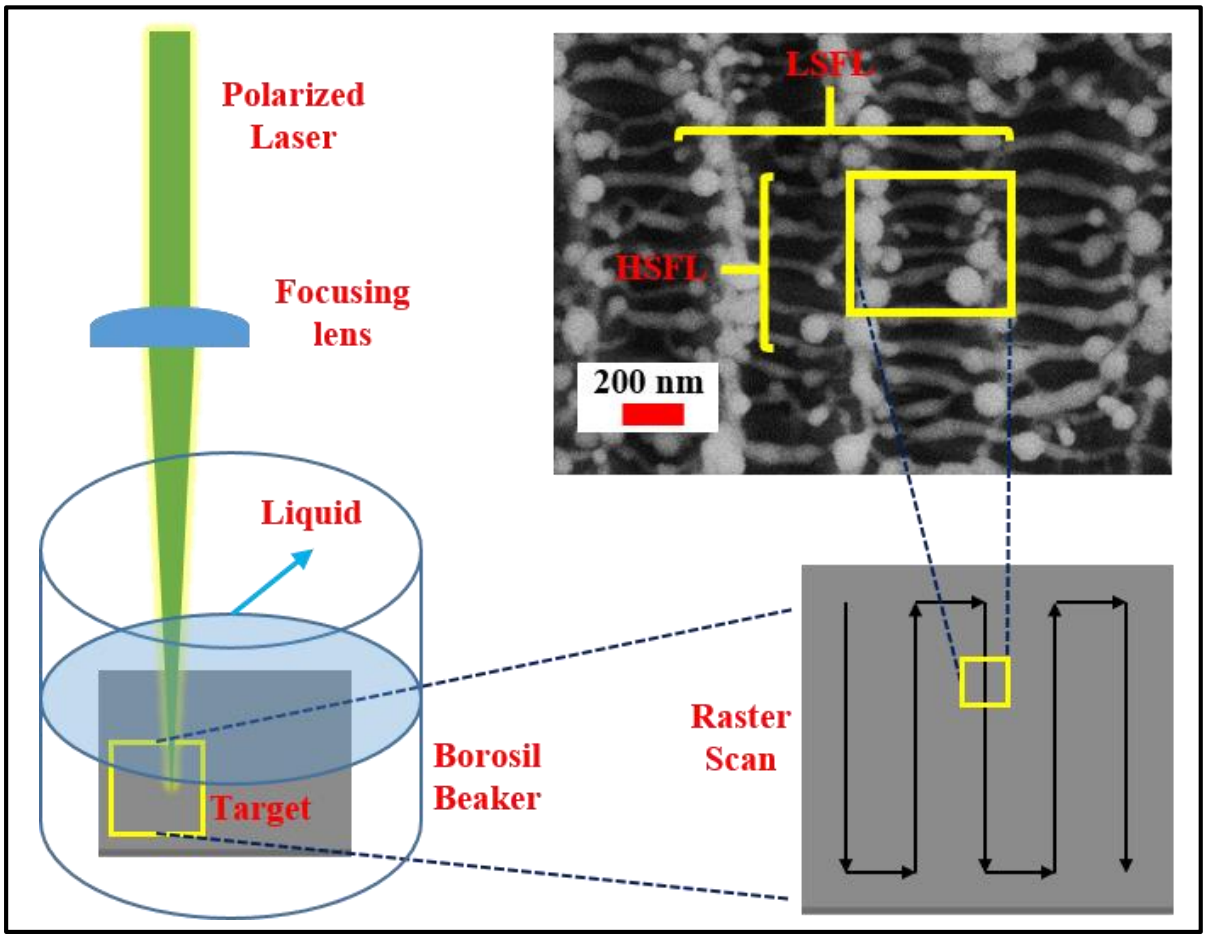

Fig 10: A schematic of the NSs fabrication by raster scanning the sample, resulting in LSFL and HSFL formation

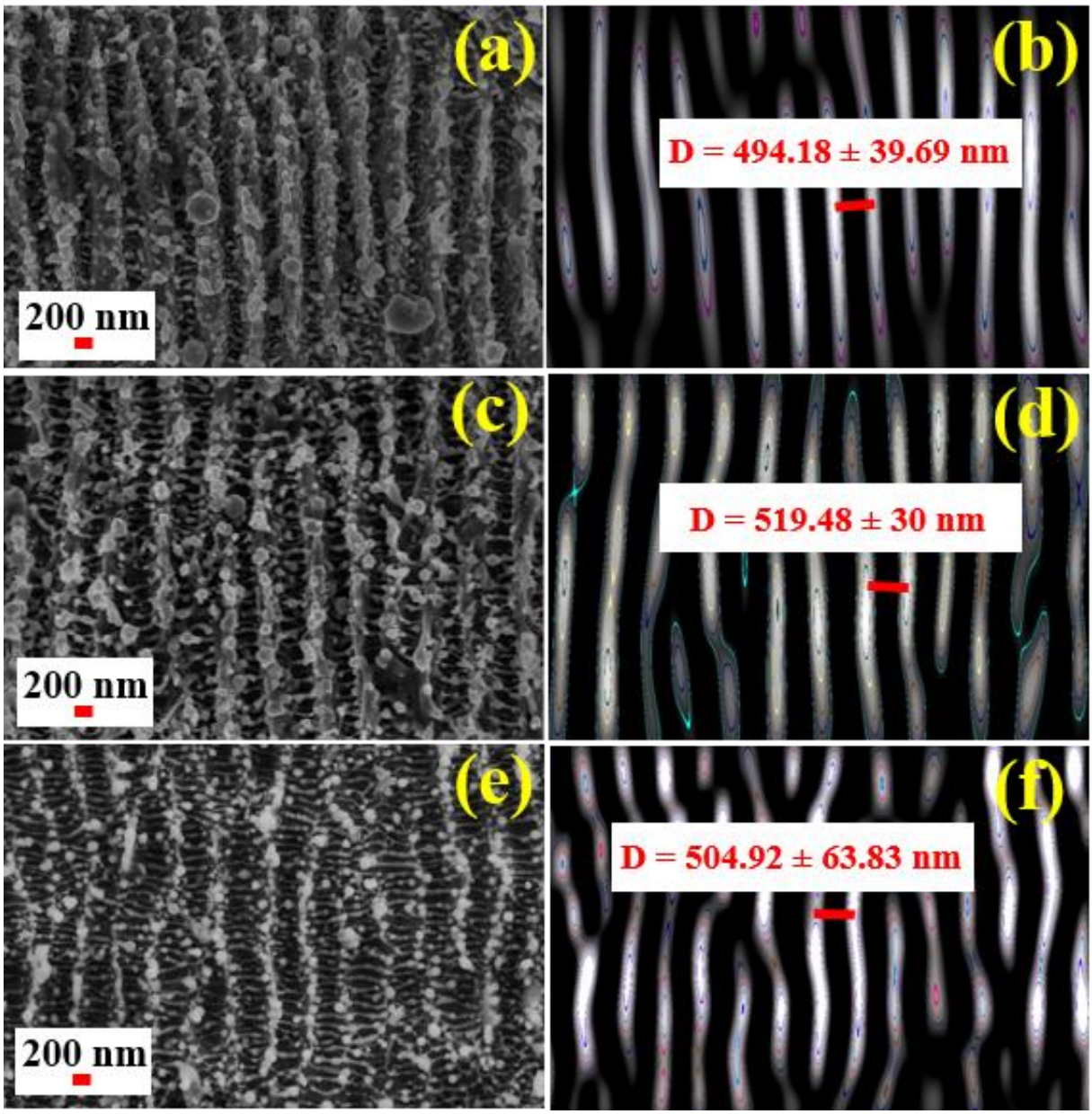

Fig 11: FESEM image and 2D FFT of LSFL with its spatial periodicity on laser ablated NSs in: (a)-(b) DW, (c)-(d) Toluene, and (e)-(f) Anisole, respectively.

Figure 13 shows the relationship between the refractive index of the liquid used for ablation and the corresponding spatial periodicity for LSFL and HSFL. The spatial periodicity of the LSFL and HSFL was observed to follow a similar trend concerning the refractive index (η) of the liquid, with spatial periodicity first increasing with the refractive index of the liquid used for LAL and then decreasing, as observed in Figures 13(a) and 13(b). The order of spatial periodicity was observed to increase from HfNSs - D (η^{DW} ~1.33 [50]) to HfNSs - T ($\eta^{Toluene}$ ~1.49 [51]) and then decrease again for HfNSs - A ($\eta^{Anisole}$ ~1.51 [52,53]). The observable pattern in HFSL size corresponding to the refractive index of the liquid may be due to the independence of HSFL from λ_L [54]. HSFL size depends on laser parameters such as fluence, energy dose, and pulse duration [55]. In the case of LSFL, further experimentation is planned to draw any conclusion regarding the relationship between the refractive index of the liquid and spatial periodicity. Re-deposition and re-solidification of the ablated NPs on NSs were also

observed, which matches with observation in an earlier reported work [56] for titanium ablation, a metal in the same group in the periodic table as Hf. These properties make Hf metal suitable for laser patterning of sub-wavelength-size structures, and the choice of Liquid for LAL gives freedom to vary the feature size. Combined with the picosecond laser's high precision processing and industrial scalability, Hf is a potential material for sophisticated design patterning [57].

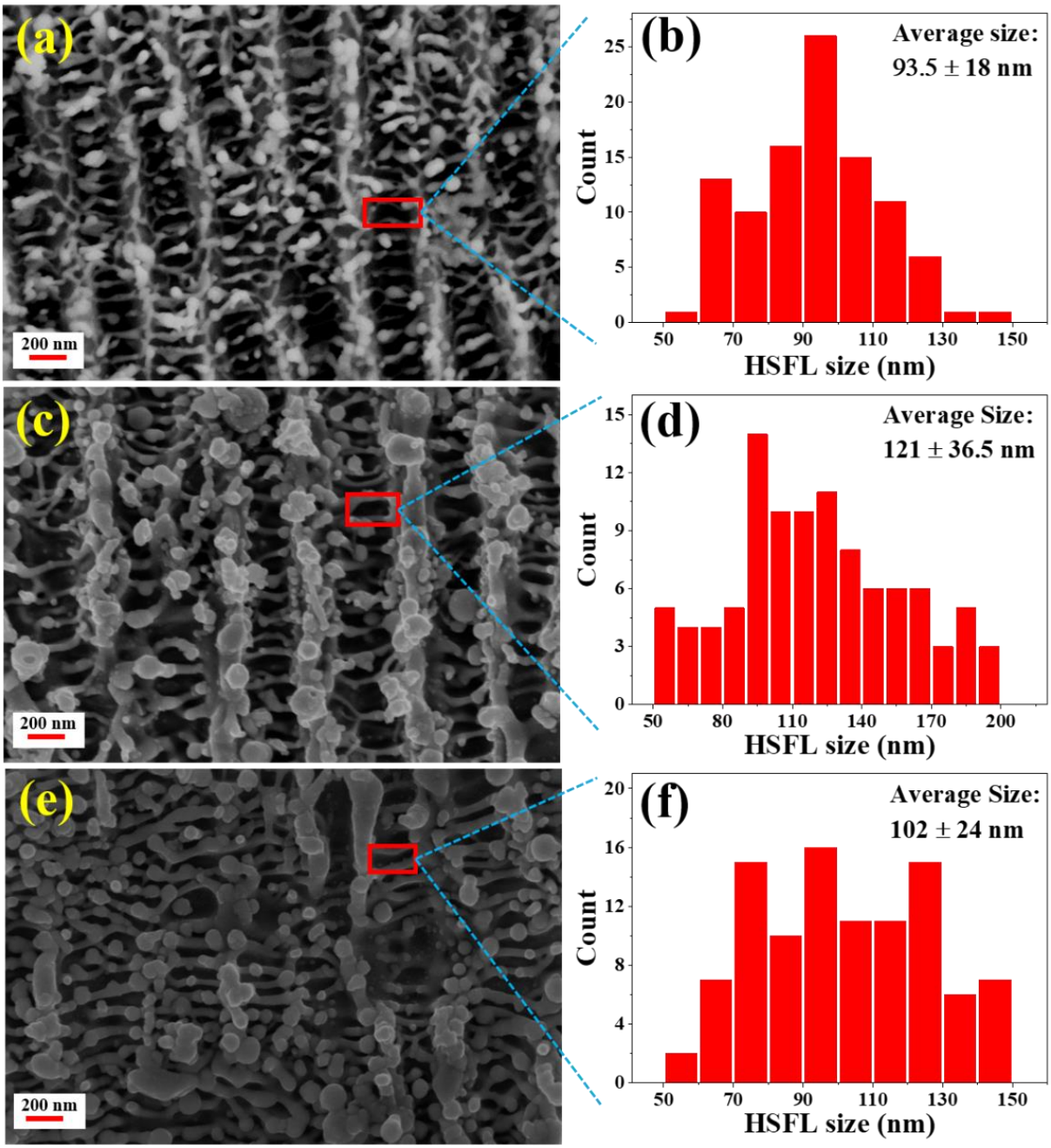

Fig 12: FESEM image and HSFL size distribution of laser ablated NSs in: (a)-(b) DW, (c)-(d) Toluene, and (e)-(f) Anisole, respectively.

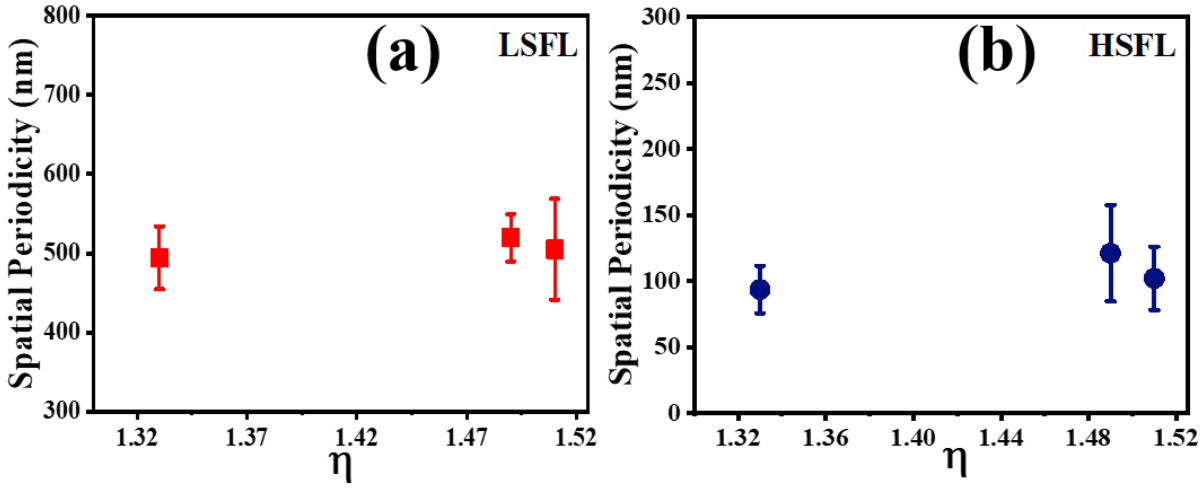

Fig 13: Effect of refractive index on spatial periodicity of (a) LSFL and (b) HSFL.

Conclusions

The current study presented that the fabrication of HfO_2 NPs and nanofibres in DW, HfC core-shell NPs with multi-layered graphitic shells in toluene and anisole was successfully achieved via LAL of Hf metal. It was observed that the obtained NPs possessed a broad size distribution. Most NPs had a diameter between ~5 nm and ~20 nm. The polycrystalline nature of HfNPs – D, HfNPs - T and HfNPs - A was found based on the obtained results. The HfO_2 nanofibers were also found to be polycrystalline, with diameters ranging from ~5 nm to ~65 nm. The NPs showed very high and broad optical absorption throughout the UV-Visible-NIR range. The maximum absorption was observed at 30° at UV (λ = 250 nm) for HfNPs – T with just 0.72 % reflection. The absorption decreases in HfNPs - D, HfNPs – T, and HfNPs – A with an increase in wavelength and angle of incidence. The successful fabrication of Hf NSs with the formation of LIPSS with LSFL and HSFL orthogonal was also demonstrated. The LSFL and HSFL both showed quasi-periodicity. The spatial periodicity of the LSFL and HSFL followed a similar trend of first increasing and then decreasing with respect to the refractive index of the liquid used during ablation.

Acknowledgements

We acknowledge the School of Physics, the Central Facility for Nanotechnology (CNF), and the School of Chemistry for providing access to the necessary instruments. Venugopal Rao Soma acknowledges financial support from DRDO, India, through ACRHEM. We thank IOE and UOH for their financial support [Ref. No. UOH/IOE/RC1/RC1- 20-016].

Funding

Funding is provided by IOE, UoH and ACRHEM/DRDO. CSIR funded Mangababu using a NET-JRF. S.V.S Nageswara Rao DST PURSE, UGC-SAP-DRS-1, CASEST, and SOP for financial support and CFN, UGC-NRC S. Venugopal Rao thanks DRDO, India for financial support through ACRHEM [[#ERIP/ ER/1501138/M/01/319/D(R&D)].

Data Availability

This article includes all the data and figures used for analysis.

Declaration

Conflict of Interest

The author declares there is no conflict of interest.

References

(1) Wan, Y.; Zhou, X. *RSC Adv.* **2017**, *7*, 7763–7773. doi:10.1039/C6RA26663K

(2) Araiza, J. de J.; Álvarez-Fraga, L.; Gago, R.; Sánchez, O. *Materials (Basel).* **2023**, *16*, 5331. doi:10.3390/ma16155331

(3) Bokhonov, B. B.; Dudina, D. V. *Ceram. Int.* **2017**, *43*, 14529–14532. doi:10.1016/j.ceramint.2017.07.164

(4) Zagorac, J.; Schön, J. C.; Matović, B.; Butulija, S.; Zagorac, D. *Crystals* **2024**, *14*, 340. doi:10.3390/cryst14040340

(5) Ulybkin, A.; Rybka, A.; Kovtun, K.; Kutny, V.; Voyevodin, V.; Pudov, A.; Azhazha, R. *Nucl. Eng. Technol.* **2019**, *51*, 1964–1969. doi:10.1016/j.net.2019.06.007

(6) Zhang, J.; Claverie, J.; Chaker, M.; Ma, D. *ChemPhysChem* **2017**, *18*, 986–1006. doi:10.1002/cphc.201601220

(7) Cotton, S. A. *Annu. Reports Sect. "A" (Inorganic Chem.* **2008**, *104*, 145. doi:10.1039/b716569m

(8) Skrodzki, D.; Molinaro, M.; Brown, R.; Moitra, P.; Pan, D. *ACS Nano* **2024**, *18*, 1289–1324. doi:10.1021/acsnano.3c08917

(9) Khan, I.; Saeed, K.; Khan, I. *Arab. J. Chem.* **2019**, *12*, 908–931. doi:10.1016/j.arabjc.2017.05.011

(10) Scher, J. A.; Elward, J. M.; Chakraborty, A. *J. Phys. Chem. C* **2016**, *120*, 24999–25009. doi:10.1021/acs.jpcc.6b06728

(11) Kumar, S.; Bhushan, P.; Bhattacharya, S. *Fabrication of Nanostructures with Bottom-up Approach and Their Utility in Diagnostics, Therapeutics, and Others*; 2018. doi:10.1007/978-981-10-7751-7_8

(12) Abid, N.; Khan, A. M.; Shujait, S.; Chaudhary, K.; Ikram, M.; Imran, M.; Haider, J.; Khan, M.; Khan, Q.; Maqbool, M. *Adv. Colloid Interface Sci.* **2022**, *300*, 102597. doi:10.1016/j.cis.2021.102597

(13) Balachandran, A.; Sreenilayam, S. P.; Madanan, K.; Thomas, S.; Brabazon, D. *Results Eng.* **2022**, *16*, 100646. doi:10.1016/j.rineng.2022.100646

(14) Byram, C.; Moram, S. S. B.; Banerjee, D.; Beeram, R.; Rathod, J.; Soma, V. R. *J. Opt.* **2023**, *25*,

043001. doi:10.1088/2040-8986/acbc31

(15) Kolahalam, L. A.; Kasi Viswanath, I. V.; Diwakar, B. S.; Govindh, B.; Reddy, V.; Murthy, Y. L. N. *Mater. Today Proc.* **2019**, *18*, 2182–2190. doi:10.1016/j.matpr.2019.07.371

(16) Fazio, E.; Gökce, B.; De Giacomo, A.; Meneghetti, M.; Compagnini, G.; Tommasini, M.; Waag, F.; Lucotti, A.; Zanchi, C. G.; Ossi, P. M.; Dell'Aglio, M.; D'Urso, L.; Condorelli, M.; Scardaci, V.; Biscaglia, F.; Litti, L.; Gobbo, M.; Gallo, G.; Santoro, M.; Trusso, S.; Neri, F. *Nanomaterials* **2020**, *10*, 2317. doi:10.3390/nano10112317

(17) Altuwirqi, R. M.; Albakri, A. S.; Al-Jawhari, H.; Ganash, E. A. *Optik (Stuttg).* **2020**, *219*, 165280. doi:10.1016/j.ijleo.2020.165280

(18) Banerjee, D.; Moram, S. S. B.; Byram, C.; Rathod, J.; Jena, T.; Podagatlapalli, G. K.; Soma, V. R. *Appl. Surf. Sci.* **2021**, *569*, 151070. doi:10.1016/j.apsusc.2021.151070

(19) Xiao, J.; Liu, P.; Wang, C. X.; Yang, G. W. *Prog. Mater. Sci.* **2017**, *87*, 140–220. doi:10.1016/j.pmatsci.2017.02.004

(20) Aliofkhazraei, M. *Handbook of Nanoparticles*; Aliofkhazraei, M., Ed.; Springer International Publishing: Cham, 2016. doi:10.1007/978-3-319-15338-4

(21) D'Urso, L.; Spadaro, S.; Bonsignore, M.; Santangelo, S.; Compagnini, G.; Neri, F.; Fazio, E. *EPJ Web Conf.* **2018**, *167*, 04008. doi:10.1051/epjconf/201816704008

(22) Fazio, E.; Santoro, M.; Lentini, G.; Franco, D.; Guglielmino, S. P. P.; Neri, F. *Colloids Surfaces A Physicochem. Eng. Asp.* **2016**, *490*, 98–103. doi:10.1016/j.colsurfa.2015.11.034

(23) Yang, S.; Zeng, H.; Zhao, H.; Zhang, H.; Cai, W. *J. Mater. Chem.* **2011**, *21*, 4432. doi:10.1039/c0jm03475d

(24) Zhang, D.; Wada, H. *Handb. Laser Micro-and Nano-Engineering* **2021**, *3*, 1481–1516. doi:10.1007/978-3-030-63647-0_30

(25) Kuladeep, R.; Jyothi, L.; Prakash, P.; Mayank Shekhar, S.; Durga Prasad, M.; Narayana Rao, D. *J. Appl. Phys.* **2013**, *114*. doi:10.1063/1.4852976

(26) Vutova, K.; Vassileva, V.; Ratheesh, R.; Reddy, R. C.; Kumar, A. *J. Phys. Conf. Ser.* **2023**, *2443*, 012013. doi:10.1088/1742-6596/2443/1/012013

(27) Mangababu, A.; Sianglam, C.; Chandu, B.; Avasthi, D. K.; Rao, S. V.; Motapothula, M.; Rao, S. V. S. N. *J. Electron. Mater.* **2021**, *50*, 1742–1751. doi:10.1007/s11664-020-08610-z

(28) Zhang, D.; Zhang, C.; Liu, J.; Chen, Q.; Zhu, X.; Liang, C. *ACS Appl. Nano Mater.* **2019**, *2*, 28–39. doi:10.1021/acsanm.8b01541

(29) De Bonis, A.; Curcio, M.; Santagata, A.; Galasso, A.; Teghil, R. *Nanomaterials* **2020**, *10*, 145. doi:10.3390/nano10010145

(30) De Bonis, A.; Santagata, A.; Galasso, A.; Laurita, A.; Teghil, R. *J. Colloid Interface Sci.* **2017**, *489*, 76–84. doi:10.1016/j.jcis.2016.08.078

(31) Lavakusa, B.; Mohan, B. S.; Prasad, P. D.; Belachew, N.; Basavaiah, K. *Int. J. Adv. Res.* **2017**, *5*, 405–412. doi:10.21474/IJAR01/3526

(32) MOOSA, A. A.; ABED, M. S. *TURKISH J. Chem.* **2021**, *45*, 493–519. doi:10.3906/kim-2101-19

(33) Davari, S. A.; Gottfried, J. L.; Liu, C.; Ribeiro, E. L.; Duscher, G.; Mukherjee, D. *Appl. Surf. Sci.* **2019**, *473*, 156–163. doi:10.1016/j.apsusc.2018.11.238

(34) Baimler, I. V.; Lisitsyn, A. B.; Gudkov, S. V. *Front. Phys.* **2020**, *8*, 1–6. doi:10.3389/fphy.2020.620938

(35) Venkatakrishnan, K.; Vipparty, D.; Tan, B. *Opt. Express* **2011**, *19*, 15770. doi:10.1364/oe.19.015770

(36) Wang, C. X.; Liu, P.; Cui, H.; Yang, G. W. *Appl. Phys. Lett.* **2005**, *87*, 1–3. doi:10.1063/1.2132069

(37) Karatutlu, A.; Barhoum, A.; Sapelkin, A. Theories of Nanoparticle and Nanostructure Formation in Liquid Phase. In *Emerging Applications of Nanoparticles and Architecture Nanostructures*; Elsevier, 2018; pp 597–619. doi:10.1016/B978-0-323-51254-1.00020-8

(38) Thanh, N. T. K.; Maclean, N.; Mahiddine, S. *Chem. Rev.* **2014**, *114*, 7610–7630. doi:10.1021/cr400544s

(39) Singh, M. R.; Ramkrishna, D. *Chem. Eng. Sci.* **2014**, *107*, 102–113. doi:10.1016/j.ces.2013.11.047

(40) Gránásy, L.; Pusztai, T.; Börzsönyi, T.; Warren, J. A.; Douglas, J. F. *Nat. Mater.* **2004**, *3*, 645–650. doi:10.1038/nmat1190

(41) Vollath, D. *Beilstein J. Nanotechnol.* **2020**, *11*, 854–857. doi:10.3762/bjnano.11.70

(42) Durán-Olivencia, M. A.; Otálora, F. *J. Cryst. Growth* **2013**, *380*, 247–255.

doi:10.1016/j.jcrysgro.2013.06.035

(43) Liang, S.-X.; Zhang, L.-C.; Reichenberger, S.; Barcikowski, S. *Phys. Chem. Chem. Phys.* **2021**, *23*, 11121–11154. doi:10.1039/D1CP00701G

(44) Pola, J.; Urbanová, M.; Bastl, Z.; Plzák, Z.; Šubr, J.; Vorlíček, V.; Gregora, I.; Crowley, C.; Taylor, R. *Carbon N. Y.* **1997**, *35*, 605–611. doi:10.1016/S0008-6223(97)00007-9

(45) Glynn, P. D.; Reardon, E. J.; Plummer, L. N.; Busenberg, E. *Geochim. Cosmochim. Acta* **1990**, *54*, 267–282. doi:10.1016/0016-7037(90)90317-E

(46) Shaymardanov, Z.; Shaymardanova, B.; Kulenova, N. A.; Sadenova, M. A.; Shushkevich, L. V.; Charykov, N. A.; Semenov, K. N.; Keskinov, V. A.; Blokhin, A. A.; Letenko, D. G.; Kuznetsov, V. V.; Sadowski, V. *Processes* **2022**, *10*, 2493. doi:10.3390/pr10122493

(47) Feizi Mohazzab, B.; Jaleh, B.; Kakuee, O.; Fattah-alhosseini, A. *Appl. Surf. Sci.* **2019**, *478*, 623–635. doi:10.1016/j.apsusc.2019.01.259

(48) Gilliland, G. D. *Mater. Sci. Eng. R Reports* **1997**, *18*, 99–399. doi:10.1016/S0927-796X(97)80003-4

(49) Kirichenko, N. A.; Barmina, E. V.; Shafeev, G. A. *Phys. Wave Phenom.* **2018**, *26*, 264–273. doi:10.3103/S1541308X18040027

(50) Mitra, S. K.; Dass, N.; Varshneya, N. C. *J. Chem. Phys.* **1972**, *57*, 1798–1799. doi:10.1063/1.1678479

(51) Debenham, M.; Dew, G. D. *J. Phys. E.* **1981**, *14*, 544–545. doi:10.1088/0022-3735/14/5/004

(52) Al-Jimaz, A. S.; Al-Kandary, J. A.; Abdul-latif, A.-H. M.; Al-Zanki, A. M. *J. Chem. Thermodyn.* **2005**, *37*, 631–642. doi:10.1016/j.jct.2004.09.021

(53) Al-Kandary, J. A.; Al-Jimaz, A. S.; Abdul-Latif, A.-H. M. *J. Chem. Eng. Data* **2006**, *51*, 99–103. doi:10.1021/je0502546

(54) Vlahou, M.; Fraggelakis, F.; Manganas, P.; Tsibidis, G. D.; Ranella, A.; Stratakis, E. *Nanomaterials* **2022**, *12*. doi:10.3390/nano12040623

(55) Nathala, C. S. R.; Ajami, A.; Ionin, A. A.; Kudryashov, S. I.; Makarov, S. V; Ganz, T.; Assion, A.; Husinsky, W. *Opt. Express* **2015**, *23*, 5915. doi:10.1364/OE.23.005915

(56) Dar, M. H.; Kuladeep, R.; Saikiran, V.; Rao, N. D. *Appl. Surf. Sci.* **2016**, *371*, 479–487.

doi:10.1016/j.apsusc.2016.03.008

(57) Rivera, L. P.; Munoz-Martin, D.; Chávez-Chávez, A.; Morales, M.; Gómez-Rosas, G.; Molpeceres, C. *Mater. Sci. Eng. B* **2021**, *273*. doi:10.1016/j.mseb.2021.115393